Remote Sensing of Environment 344 (2026) 115542

Contents lists available at ScienceDirect

Remote Sensing of Environment

journal homepage: www.elsevier.com/locate/rse

First multi-sensor characterization of fire-emitted potassium spectral signatures from space in low-light and daytime conditions

William Julstrom[a,*], Jun Wang[a,*], Meng Zhou[a,b]

[a] Department of Chemical and Biochemical Engineering, University of Iowa, Iowa City, IA 52242, USA
[b] Goddard Earth Sciences Technology and Research (GESTAR) II, University of Maryland – Baltimore County, Baltimore, MD 21228, USA

ARTICLE INFO

Edited by Menghua Wang

Keywords:
Biomass burning
Hyperspectral imaging
TROPOMI
OCO-2
MODIS
VIIRS
Principal component analysis

ABSTRACT

The spectrum of burning biomass contains prominent potassium (K) emission lines at 766.7 nm and 770.1 nm. These emission lines are unique to flaming combustion, potentially allowing their use in development of remote sensing techniques to characterize fire phase, flaming temperature, and allow more accurate estimates of fire emissions. Previous studies have shown modest success in detecting potassium emission lines (K-lines) using airborne instruments or meter-scale spatial resolution satellites. This study, for the first time, shows the detection of K-lines in wildfire spectra under low-light conditions using the TROPOspheric Monitoring Instrument (TROPOMI), and under local noon daylight conditions using the Orbiting Carbon Observatory-2 (OCO-2). Our observations clearly show separation of dual K-line peaks and that the line at 766.7 nm (not 770.1 nm) is attenuated strongly by oxygen absorption, in contrast with previous studies. We also show that K-lines can be isolated from the background signal and atmospheric effects using Principal Component Analysis (PCA) and that the magnitude of the Principal Component (PC) corresponding to the K-lines correlates well with both fire Visible Light Power (VLP) and Fire Radiative Power (FRP) as shown by the VIIRS FIre Light Detection Algorithm (FILDA), with VLP showing better correlation. This suggests quantitatively that K-lines could add critical information to improve existing active fire algorithms for deriving a daytime fire combustion efficiency and other characteristics to better estimate fire emissions.

1. Introduction

Fires and biomass burning are important factors in global atmospheric chemistry (Crutzen et al., 1979), making their accurate detection and characterization a significant goal of atmospheric remote sensing. A key factor that determines the chemical and aerosol species emitted by fires is the phase of combustion (flaming or smoldering) or quantitatively, the combustion efficiency. The chemical species emitted by fires depends strongly on the modified combustion efficiency, defined and measured as the ratio of CO_2 to the sum of CO_2 and CO emitted. For example, only a few percent of the emissions of flaming combustion is CO, while in smoldering combustion it can be as high as 20% (Crutzen and Andreae, 1990). However, many current fire emission inventories (GFAS, FLAMBE, GFED) (Kaiser et al., 2012; Reid et al., 2009; van der Werf et al., 2017) typically use the mean or median statistics of emission factors derived from laboratory or field observations, and such statistics are typically analyzed as a function of limited biomass types (Akagi et al., 2011; Andreae, 2019; Andreae and Merlet, 2001). As a result, for the same biome type, the emission factors are often prescribed as constant in these inventories, without consideration of combustion efficiency or fire phase, leading to uncertainties in emission estimates (van der Werf et al., 2017).

The spectrum of burning biomass contains prominent emission lines at 766.7 nm and 770.11 nm due to thermally excited potassium (K) atoms released during the burning process (Vodacek et al., 2002). At the maximum of smoldering combustion in wildfires (<850 K (Kaufman et al., 1998)), elemental K, which is the species responsible for K-lines, is not emitted during the char burning phase of combustion (Sorvajarvi et al., 2014). Additionally, assuming a Boltzmann distribution, there are $\sim 4 \times 10^5$ times as many K atoms in the excited state that gives rise to the 770.11 nm emission line at 1000 K than at 600 K, which are the temperatures for flaming and smoldering combustion respectively (Kaufman et al., 1998). As such, the presence of K-lines is specific to flaming combustion (Vodacek et al., 2002). This specificity could be leveraged to provide estimations of combustion efficiency. The line-shape and center wavelength of K-lines are also sensitive pressure and

* Corresponding authors.
E-mail addresses: william-julstrom@uiowa.edu (W. Julstrom), jun-wang-1@uiowa.edu (J. Wang).

https://doi.org/10.1016/j.rse.2026.115542
Received 22 November 2025; Received in revised form 5 June 2026; Accepted 18 June 2026
Available online 28 June 2026

temperature (Ding et al., 2022) and could therefore be leveraged by an instrument with sufficient sensitivity.

Here, we explore the feasibility of detecting fire-emitted K-lines quantitatively from space-borne instruments in daytime conditions. Past case studies have demonstrated modest success in the detection and utilization of K-lines in fire spectra, primarily through airborne instruments. These studies show that K-line signals associated with the flaming fires are discernable from the meter-scale spatial resolution airborne (Amici et al., 2011; Dennison and Roberts, 2009; Ononye et al., 2005; Owsley-Brown et al., 2024; Vodacek et al., 2002) and satellite (Amici et al., 2011; Waigl et al., 2019) hyperspectral instruments, and contributes to the increase of intensity in Near InfraRed (NIR) broadband-based airborne fire detection (Kaaret et al., 2022). However, past K-line detections tend to only detect the most intense flaming pixels, underperforming other fire detection methods likely due to the low spectral resolution (~10 nm) of the observing instruments and attenuation by smoke (Dennison and Roberts, 2009; Waigl et al., 2019). Despite underperforming as a fire detection method, K-lines show great potential for characterizing fire emissions. Using a K-line-based hyperspectral index developed by Amici et al. (2011), and in conjunction with FRP measurements, Owsley-Brown et al. (2024) was able to derive fire phase-dependent emission factors and modified combustion efficiency (MCE) in laboratory fires and applied these to estimate fire emissions using airborne data. While this method has not been extended to satellite data, it demonstrates the potential of K-lines as a tool complementary to existing remote sensing techniques for estimating fire emissions from space.

For satellite remote sensing of K-lines, hyperspectral resolution is needed because of several factors which either weaken or overwhelm the observable signal. These include: oxygen-A band absorption of the 766.7 nm K-line (Magidimisha and Griffith, 2017), radiative attenuation by smoke, and the comparatively strong solar signal. It has been suggested (Amici et al., 2011; Vodacek et al., 2002) that fine spectral resolution on the order of <0.5 nm is required to resolve the signal of K-lines from space.

This work differs from past studies by taking advantage of newer hyperspectral spaceborne instruments with significantly improved spectral resolution. For the first time, with a multiple sensor approach, we show here that K-lines are detectable quantitatively under low-light conditions (from the TROPOMI instrument) and daytime local-noon observations (from the OCO-2 instrument). Using Principal Component Analysis (PCA), we isolate the K-line spectral signature for both instruments and show that the Principal Component (PC) containing the K-lines correlates well with Fire Radiative Power (FRP) and Visible Light Power (VLP), with VLP showing the strongest correlation. These results demonstrate the detectability of K-lines using TROPOMI and OCO-2 and their sensitivity to flaming combustion, opening a pathway to space-based characterization of flaming phase of wildfires and their emissions in future studies.

2. Data and methods

2.1. Hyperspectral data

We used level-1B data from two instruments capable of resolving the potassium line at high spectral resolution: the TROPOMI instrument aboard the Sentinel-5 Precursor (Sentinel-5p) satellite, launched in 2017, and OCO-2, launched in 2014. TROPOMI level-1b data have a swath width of ~2600 km and a spatial resolution of 5.5 × 3.5 km^2 at nadir, allowing for global spatial coverage across a wide range of viewing and illumination angles (Chen et al., 2021).

Band 6 data from TROPOMI is used; it has a maximum wavelength range of 725–786 nm and a spectral resolution of ~0.34 nm, much higher than those of the instruments used in previous studies. Preliminary tests showed that K-lines were not visible in the TROPOMI daytime spectra due to the high intensity and variance of sunlight. To minimize solar contamination, we use observations during the brief period in TROPOMI's orbit where it performs low-light measurements in high latitude regions after passing over the terminator line. To further limit solar contamination, only the final 200 along-track pixel rows beyond the terminator line are considered here and pixels with solar zenith angle less than 95° are masked out for quantitative comparison to VIIRS fire data. Additionally, since fewer sensor pixels are binned into each ground pixel near the edge of the swath, the 20 ground pixels closest to either edge of the TROPOMI swath were excluded from the analysis due to their low signal-to-noise ratio.

OCO-2 level-1b data have a nominal swath width of ~10 km and a spatial resolution of 1.3 × 2.3 km^2 (Crisp et al., 2017). As a sun-synchronous, predominantly nadir-viewing instrument, this limits the observations to near local noon time. We used the OCO-2 oxygen band measurements which ranges from 757.564 nm to 770.625 nm with a spectral resolution of ~0.04 nm, nearly an order of magnitude finer than TROPOMI. We show that the much higher spectral and spatial resolution of OCO-2 enables detection of fire spectral structure of K-lines during the day at local noon time.

2.2. Active fire detection data

The locations of active fires were determined using the Suomi-NPP Visible Infrared Imaging Radiometer Suite (VIIRS) FIre Light Detection Algorithm (FILDA-2) product (Zhou et al., 2023) for the low-light TROPOMI cases and the Aqua Moderate Resolution Imaging Spectroradiometer (MODIS) MYD14 thermal anomaly and fire product for the OCO-2 cases. The VNP03MOD and MYD03 geolocation products corresponding to each instrument were also used to facilitate colocation of the fire detection and hyperspectral NIR measurements.

FILDA-2 has the additional advantage of combining VIIRS Day-and-Night Band (DNB) for fire light detection and mid-wave IR and thermal channels to not only derive FRP (as in MYD03) but also the visible light power (VLP) and visible energy fraction or VEF (e.g., the ratio of VLP and FRP) for each detected active fire pixel allowing better characterization of fire flaming content (Wang et al., 2020); as such it is only available at low-light conditions. As the FILDA-2 operational product excludes measurements with a solar zenith angle less than 95°, we adjust this threshold to 92.5° to encompass several particularly intense fires in our case list, although the threshold was set to 95° for the PCA.

Suomi-NPP leads the Sentinel-5P satellite by 3.5 min and Aqua trails OCO-2 by 6 min. FILDA-2 product has a spatial resolution of 750 m and a swath width of 3060 km and the MODIS product has a spatial resolution of 1 km and a swath width of 2300 km. Hence, both VIIRS and MODIS accompany the hyperspectral TROPOMI and OCO-2 instruments, respectively, on the daily basis with nearly spatially and temporally coincident observations at the global coverage to comprehensively characterize fire emitted radiances spectrally and spatially, allowing near simultaneous detection of fires and measurement of K-lines.

2.3. Fire cases

In total, 31 coincident cases were manually selected for VIIRS-TROPOMI and MODIS-OCO-2 synergy (see table S1) with emphasis on the presumed likelihood of K-line detection. For TROPOMI, 5 cases were selected involving intense fires observable under low-light conditions, which tended to occur in late summer in Northern Siberia or Alaska. While the most intense fires were in Siberia, two Alaskan cases were selected for variety. For OCO-2, 26 cases were selected from a 4-year period where it shared the same orbit as Aqua. 20 of these cases were selected from regions prone for large fires, but five additional cases were chosen from other locations for variety. Fewer cases (days) of observations were required for TROPOMI due to its much larger swath width, which encompasses large fire regions, while for OCO-2, each case contains only 1 or (rarely) 2 fires.

2.4. Data correction and colocation

For the TROPOMI instrument, for a given hyperspectral channel, the wavelength varies with the across-track index with longer wavelengths at nadir and shorter wavelengths closer to the swath edge. This was corrected by shifting the hyperspectral channel indices such that each corrected channel contained approximately the same wavelength. The hyperspectral channel indices before and after this correction are shown in Fig. S1. After this correction, the wavelength for a given hyperspectral channel index can still vary by as much as the spectral resolution of the instrument, or ~ 0.34 nm. Because of this source of variance, the resulting spectra were then linearly interpolated to the reference wavelength array. Additionally, TROPOMI spectra with significant cosmic ray interference were removed using a median filter.

For OCO-2, a correction and interpolation scheme like what was used for TROPOMI was applied. Additionally, off-nadir OCO-2 observations have a large radial velocity component, resulting in non-negligible Doppler shifts. This was corrected before wavelength correction and interpolation according to:

$$\lambda_0 = \frac{\lambda}{1 + \frac{v_r}{c}}$$

where λ_0 is wavelength at emission, λ is the wavelength as observed by OCO-2, v_r is the radial velocity of OCO-2 relative to the fire pixel, and c is the speed of light. Like the TROPOMI correction, some variance from the correction and from the differing spectral response of each across-track pixel will be introduced into the data, but the effects from these non-idealities are minor.

Since the potassium signal is weak compared to other signals in the measured spectra, especially for the daytime noon OCO-2 measurements associated with strong solar radiation, only TROPOMI or OCO-2 pixels containing active fires were used. Pixels were classified as containing active fire if the TROPOMI or OCO-2 pixel overlapped with a VIIRS or MODIS fire detection pixel.

2.5. PCA of fire pixel spectra

PCA was used to isolate the K-line signal because it makes use of many channels to resolve the detailed spectral shape of the K-lines. This results in less sensitivity to noise and cosmic ray artifacts on any given channel. PCA can also account for mixing of the signal with oxygen absorption lines and other large sources of variance, since these are separated as distinct PCs, ensuring robustness across varying viewing and illumination angles. A simple 2-channel band difference test cannot robustly account for these interferences. The detailed shape of the K-lines may also contain additional information that a 2-channel band difference test cannot resolve.

After applying colocation and wavelength correction to the five TROPOMI cases and 26 OCO-2 cases, 3825 TROPOMI fire pixels and 1160 OCO-2 fire pixels remained. The spectra of these pixels are shown in Figs. S2 and S3. PCA was applied to the resultant spectral data of each instrument to isolate the K-line signal. In the PCA, each fire pixel's spectrum was treated as an observation vector of radiance values across spectral channels. For TROPOMI, a spectral range of 765 nm to 771 nm was used as it contains both K-lines. OCO-2 data analysis reveals that the K-line at 766.7 nm coincides directly with a strong oxygen absorption line which contaminates the observed signal. This interference combined with the strong solar background and sparser data of the OCO-2 dataset prevented clean isolation of the more attenuated 766.7 nm K-line. As such, the PCA for the OCO-2 data was performed on the spectral region from 769 nm to 771 nm containing only the 770.1 nm K-line.

3. Analysis and results

3.1. TROPOMI: common spectral signature of fire emitted K-lines in low light conditions

Fig. 1 presents the first observation of the distinct dual-peak structure of K-line spectra from space. As an example, to illustrate that K-lines can be detected under low-light conditions with TROPOMI, we show in Fig. 1 the TROPOMI NIR spectra over a particularly intense cluster of fires from a case in Siberia (Fig. 1a) on 08 August 2021. Fire NIR spectra are analyzed over the TROPOMI pixels (Fig. 1c and d) that host FILDA-2 fire pixels, while background NIR spectrum are collected from no-fire pixels (Fig. 1b). Clear K-lines with dual peaks are evident at 766.7 nm and 770.1 nm for fire pixels (Figs. 1c and d), respectively. Notably, the peak spectral radiance enhancement of the K-line at 766.7 nm is roughly equal to the line at 770.1 nm, contradicting previous studies which claim that the line at 770.1 nm would be attenuated by ~60% (Amici et al., 2011; Kaaret et al., 2022; Vodacek et al., 2002). These studies used in vacuo wavelengths for the oxygen absorption lines but in-air wavelengths for the K-lines in their radiative transfer calculations, resulting in a misalignment.

Quantitatively, the spectra of TROPOMI pixels coincident with higher FILDA-2 FRP values show more prominent K-lines. For example, the FRP of the fire pixels shown in Fig. 1c and d are 68.4 MW km^{-2} and 55.1 MW km^{-2} respectively, with Fig. 1c showing stronger intensity of K-lines and FRP. The relationship is even stronger with VLP and K-line strength as Fig. 1c and d show VLP values of 0.018 MW km^{-2} and 0.006 MW km^{-2}, respectively. These values equate to VEF values of 0.00026 and 0.00011 for the fire pixels shown in Fig. 1c and d, respectively, indicating stronger flaming in the former. This is expected since both observables are strongly correlated with fire phase. The peak spectral radiance of the K-line signal is approximately 0.3 mW m^{-2} nm^{-1} sr^{-1}, which is clearly distinguishable above the background light level, at least for large fires.

Statistically, the K-line signal can be separated from spectral variance associated with non-fire factors such as solar radiance, oxygen absorption, etc. This is demonstrated by applying PCA to the TROPOMI fire pixel spectra. Fig. 2a and b show the first two PCs, with PC-2 clearly showing the isolated K-lines, explaining 3.41% of the variance in the TROPOMI fire pixel spectra. The majority (58.22%) of the variance, captured by PC-1, is introduced by background sunlight. The remaining PCs, which account for 38.37% of the signal variance, likely capture variance introduced from the variation of surface reflection, varying hyperspectral channel center wavelengths, differences in oxygen absorption, and from the higher proportion of instrument noise in low-light conditions (Fig. S5). PC-1 shows weak K-line peaks at 766.7 nm and 770.1 nm, indicating that PC-2 may not fully capture the K-line signal, but this cross-contamination is small and not significant. As no other PCs show these features and PC-2 shows no contamination from other sources of variance, we consider PCA an effective method for isolating K-lines in wildfire spectra.

Assuming that PC-2 fully and exclusively captures the K-lines, the scores of PC-2 are proportional to the K-line radiance. To further quantify the K-line signal, we demonstrate correlation of the scores of PC-2 with respect to the FILDA-2 FRP and VLP, showing that VLP correlates more strongly than FRP. As the uncertainty of both the FRP and PC-2 scores should be considered, we use Reduced Major Axis (RMA) regression instead of Ordinary Least Squares (OLS) regression. For this analysis, we exclude TROPOMI fire pixels with PC-2 scores less than 0.01 to focus on those with distinct K-line features. Some of these excluded pixels, however, have high FRP values but no or very small K-line signal, which could be due to large smoldering fraction (and

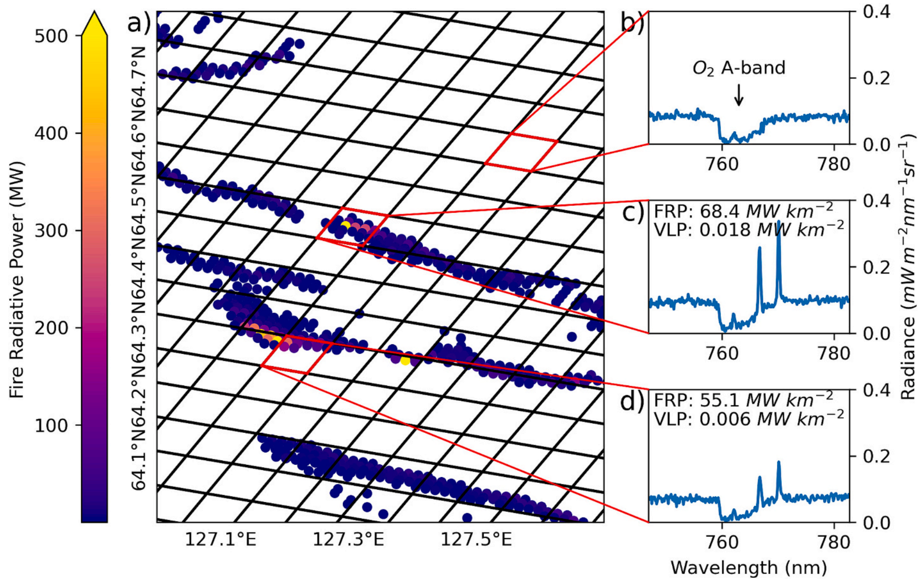

Fig. 1. FILDA-2 fire detections and TROPOMI band-6 spectra for a scene at 18:05 UTC on 2021-08-08 in Siberia. (a) FILDA-2 FRP measurements for a selected fire region with overlaid TROPOMI ground pixel footprints. (b) Measured spectrum for a background pixel, showing no potassium line detections. (c) Measured spectrum for a strong fire pixel showing K-lines with regridded FILDA-2 FRP and VLP measurements. (d) Same as (c), but for a fire pixel showing weaker K-lines.

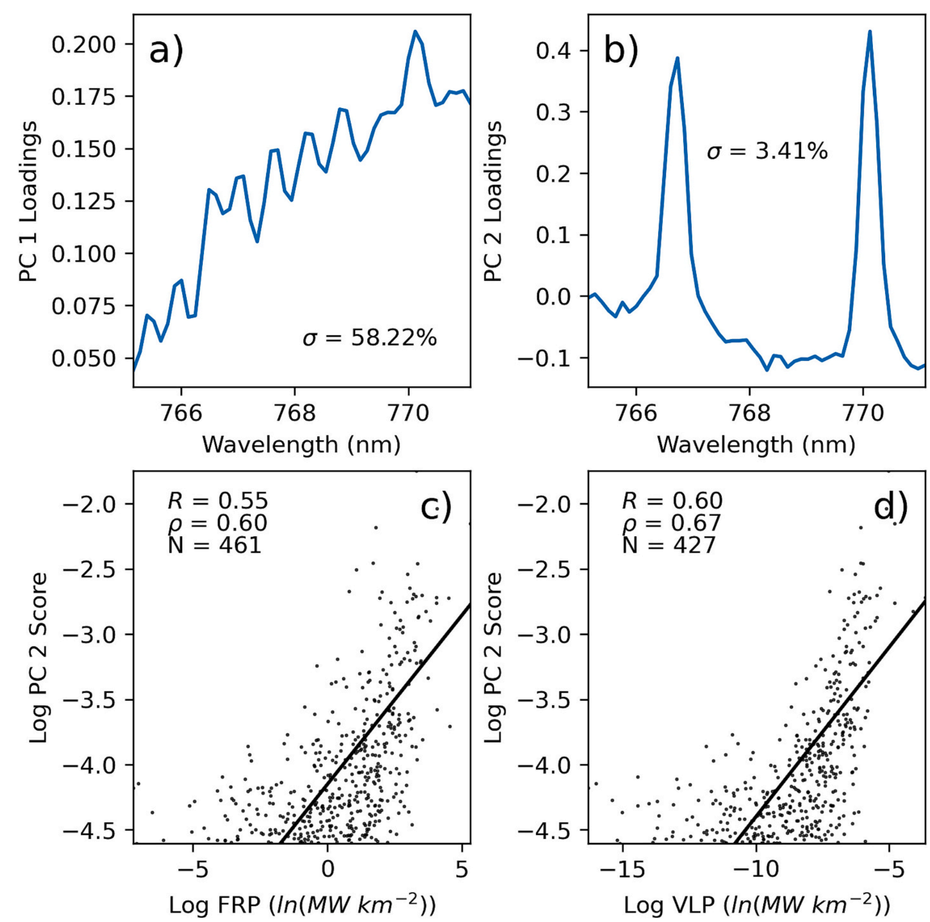

Fig. 2. a) PC-1 of the TROPOMI fire pixels in the spectral region containing both K-lines and their explained variance. b) Same but for PC-2 showing the potassium signal. c) Log-log correlation between FILDA-2 FRP and the scores of PC-2 thresholded at 0.01. d) Same but with FILDA-2 VLP. In c) and d), also denoted are the values of linear correlation coefficient R, ranked correlation coefficient (ρ), statistical significance test (p), and number of samples. Please see text for details.

possibly smoke particle attenuation) in those TROPOMI pixels, as these excluded pixels also show reduced VLP (Fig. S6). Future studies may disentangle these factors.

Potential sources of uncertainty in the scores of PC-2 include instrument radiometric error, attenuation of the signal by smoke and atmosphere, and uncertainty resulting from mixing of the K-line signal between PCs. While PCA as a technique does not provide uncertainty estimates, it may be possible to quantify uncertainty associated with the PCA decomposition using statistical techniques such as bootstrapping or cross-validation. Future studies could apply statistical techniques to estimate uncertainty in the extracted K-line signal. Additionally, a forward model based on radiative transfer modeling or empirical background fitting similar to that described in Guanter et al. (2021) could be developed to avoid uncertainty introduced by interference between PCs and provide a more physically based estimate of K-line radiance.

Figs. 2c and d show the correlation and the RMA regression line of the PC-2 scores of the TROPOMI fire pixels and FILDA-2 FRP and VLP, respectively. Both FRP ($R = 0.55$) and VLP ($R = 0.60$) show statistically significant correlation with the PC-2 scores, and therefore K-line radiance. Additionally, the Spearman rank correlation values are higher for FRP ($\rho = 0.60$) and VLP ($\rho = 0.67$), indicating stronger non-linear correlation not fully captured by linear regression. The VLP results show a stronger correlation with K-line PC scores, which is expected since VLP is a better indicator of fire phase and combustion efficiency than FRP. These results can be further improved by consideration of the attenuation of the K-line signal by smoke and by accounting for the low spatial resolution of TROPOMI which cannot easily distinguish regions of flaming and smoldering combustion. A future instrument with higher spatial resolution or a more sophisticated retrieval algorithm could accomplish this. Additionally, the VLP and FRP measurements may themselves be subject to atmospheric attenuation (Deng et al., 2024) and atmospheric correction of these measurements may improve these results.

Geographically, when a PCA transformation is applied to the whole TROPOMI swath using the previously calculated PCs, the locations and magnitudes of PC-2 values correspond well qualitatively with the locations and magnitudes of FILDA-2 VLP values. As an example, Fig. 3a and b show the spatial distribution of PC scores and FILDA-2 VLP, respectively, while Fig. 3c and d show a zoomed-in subset area of 3a and 3b, correspondingly. High PC-2 values correspond to high FILDA-2 VLP values and, in general, these two spatial distributions are in good agreement. Fig. 3c and d provide a closer view for comparison, in which those fire areas with high VLP values are also the areas with high PC-2 scores. Note, for the comparison, the FILDA VLPs were resampled to the TROPOMI pixel grid box and weighted by area. Quantitatively, the variation or ratio between VLP and PC-2 scores is not necessarily constant, which is understood, because their correlations, while significant, has R of 0.60 (Fig. 2).

Indeed, the K-line PC scores in the TROPOMI swath are noisy, with many pixels that lack FILDA-2 fire detections still possessing small, non-zero PC-2 scores. This is illustrated in Fig. 3a and c. As such, for quantitative detection of TROPOMI pixels with significant fraction of flaming fires, a threshold to filter those noisy pixels is useful. As shown in Fig. 3e, a K-line PC score threshold of ~0.05 minimizes the false alarm rate (defined as the ratio of above-threshold K-line detections that do not coincide with VIIRS fire detections), resulting in roughly 15% of above-threshold values falling outside of fire pixels. While this threshold minimizes the number of K-line detections outside of VIIRS fire

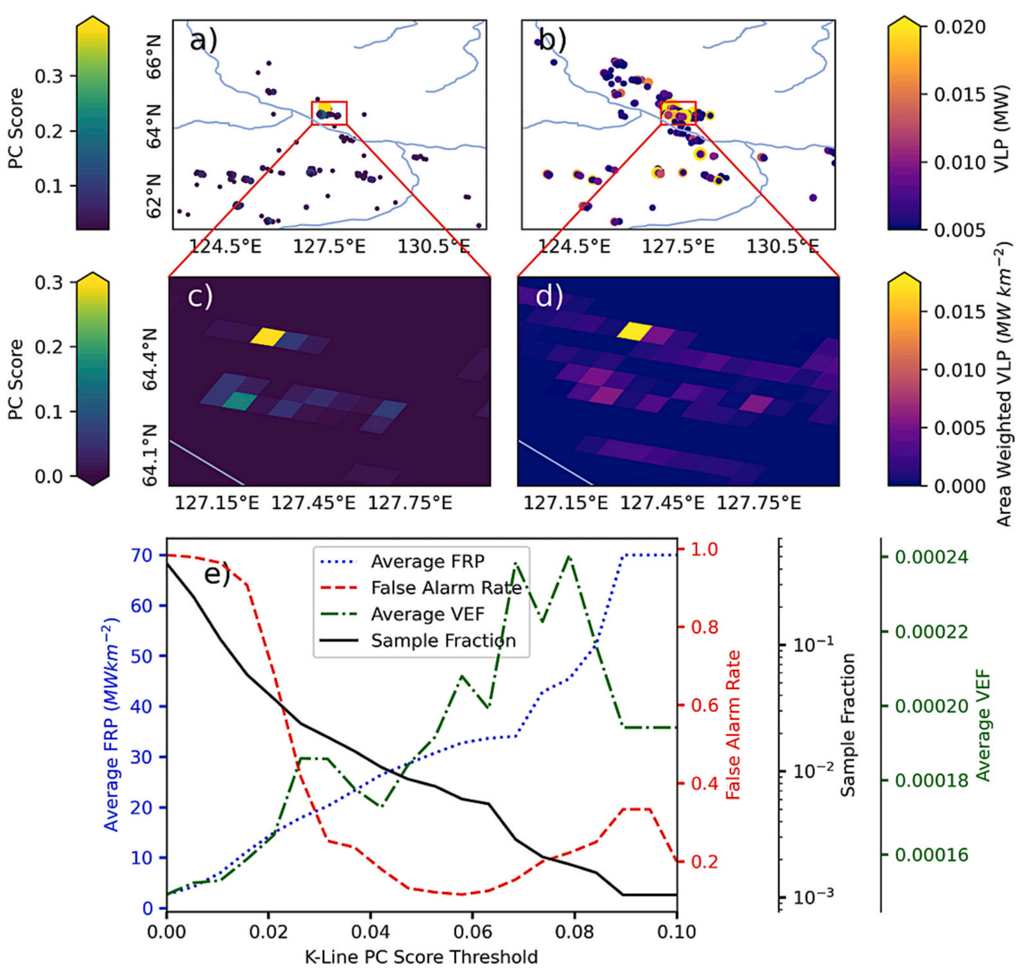

Fig. 3. Comparison between geolocated PC-2 scores and FILDA-2 VLP measurements. (a) spatial distribution of PC-2 scores in a region surrounding the domain shown in Fig. 1 with threshold at 0.02 applied for the PC-2 score value. (b) FILDA-2 VLP measurements for the same region and with a threshold of 0.005 MW applied. (c) A zoomed-in view of a portion of (a). (d) A zoomed in view of a portion of (b) but with FILDA-2 VLP resampled to the TROPOMI grid. (e) Relationship between mean values of FRP, VEF, sample fraction and false alarm rate for the study domain as a function of threshold value (x-axis) used for K-Line PC-2 scores.

detections, the sample fraction (defined as the fraction of VIIRS fire pixels containing K-line detections above this threshold) is very small (~1%). As shown in Fig. 3a and c, a large number of genuine K-line detections fall are excluded in this threshold, so there is a tradeoff between noise removal and flaming fire detection. Additionally, the mean FRP and VEF of fire pixels containing the thresholded K-line detections increase consistently with increasing K-line PC thresholds (Fig. 3e) indicating that higher thresholds isolate the more intense and flaming fire pixels.

These results – that the K-line signal is sensitive to flaming combustion and that higher K-line threshold isolate intense, flaming combustion – imply that K-line observations could be leveraged in conjunction with FRP measurements to aid in determining the degree of flaming combustion. This relationship is currently not known, but future work could relate these observations to empirical emission data or thermodynamic model results to estimate combustion efficiency.

3.2. OCO-2 noontime fire spectral signature of potassium line

OCO-2 is capable of directly measuring K-lines at local noon time in mid-latitude regions. As an example, Fig. 4b shows the spectra difference between a fire and background pixel, as identified based on MODIS fire detection and FRP (Fig. 4a). The difference is shown because the K-lines are much less clear in the raw spectra (Fig. S8). This unprecedented capability of detection is made possible by the ultra-fine spectral resolution (0.04 nm) and spatial resolution (1.3 km × 2.3 km) of OCO-2 which are a factor of 8 finer and a factor of 6 smaller than those of TROPOMI, respectively. As a result, it is not constrained by the same low-light requirement as TROPOMI, allowing greater geographical coverage at daytime, for detecting K-lines. Indeed, due to the high spectral resolution, oxygen absorption line contamination of the 766.7 nm line and the Voigt line shape of both K-lines is also clearly visible in the OCO-2 measurements (Fig. 4b). The ability of OCO-2 to resolve these fine details may be leveraged by a future algorithm to retrieve additional fire information since some, such as line width, are sensitive to fire temperature (Ding et al., 2022). The peak spectral radiance of the 770.1 nm K-line peak is ~45 $mWm^{-2}nm^{-1}sr^{-1}$, which is much larger than the corresponding ~0.3 $mWm^{-2}nm^{-1}sr^{-1}$ measured by TROPOMI. This discrepancy is likely because of OCO-2's much higher spatial resolution, which allows higher flaming pixel fraction, spectral resolution, so the peak appears sharper, and the fact that fires burn at much higher intensity during daytime hours.

Performing PCA on the OCO-2 fire pixels successfully isolates the K-line signal as PC-2 (Fig. 4c). PC-2 is somewhat contaminated by nearby oxygen absorption lines, a consequence of the somewhat sparse data and strong solar signal, but overall, the K-line signal is very clear. Additionally, there is no sign of K-line contamination in any of the other first six PCs (Fig. S7) indicating that PCA is excellent at isolating the signal. The high spectral resolution of OCO-2 is responsible for this success as it is able to distinguish individual oxygen absorption lines, unlike TROPOMI. After removing the PC capturing solar variance, the K-line PC in the OCO-2 PCA makes up 8.55% (Fig. 4c) of the total variance in the observed fire pixel spectra. These results clearly demonstrate the feasibility of daytime observations of K-lines using satellite remote sensing.

Despite the successes of OCO-2 in isolating the K-lines, the resulting K-line PC shows weaker correlation with MODIS FRP ($R = 0.38$, $\rho = 0.49$) (Fig. 4d) than the TROPOMI results with FILDA-2 products. This poor performance compared to the TROPOMI results is mainly due to the intense background solar signal which makes up >99.9% of the variance of the unprocessed fire pixel spectra and easily overwhelms the weak K-line signal. Using PCA, however, is intended as a proof-of-concept for the isolation of K-lines in wildfire spectra at local noon time. More sophisticated retrieval algorithms using radiative transfer modeling are likely to improve these results.

4. Summary and conclusions

Using a multiple sensor approach, this study demonstrates for the first time that the K-lines at 766.7 nm and 770.1 nm are readily measurable in both low-light (dawn or dusk) and noon conditions from TROPOMI and OCO-2 respectively. This study is also the first to show measurements of the individual K-line peaks due to the high spectral resolution of the instruments used. In contrast to previous studies, we show that the K-line at 766.7 nm is attenuated by oxygen absorption

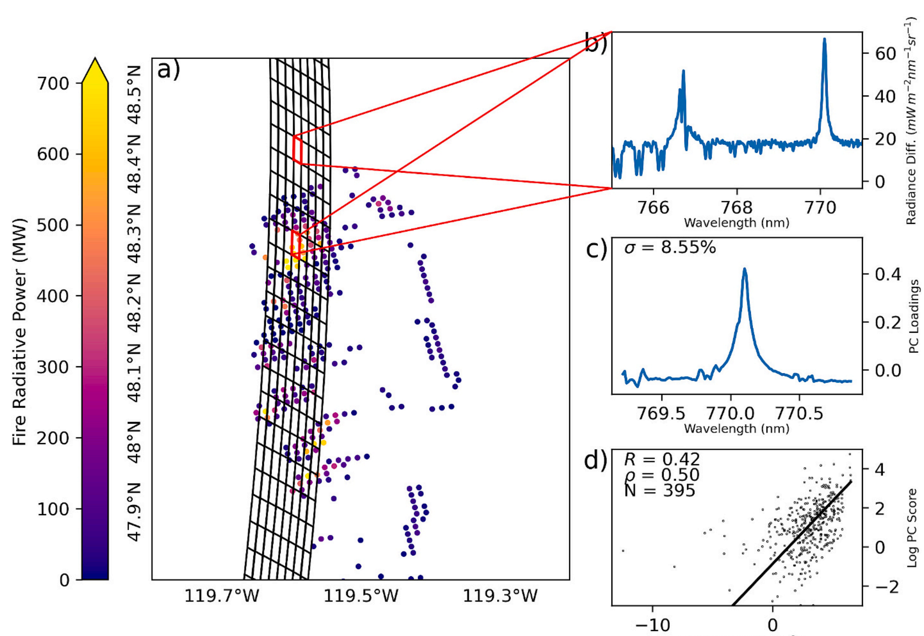

Fig. 4. Daytime MODIS fire detections and OCO-2 O_2-band spectra for a fire at 20:56 UTC (13:56 PDT) on 2020-09-07 at 48.1 N 119.5 W with a solar zenith angle of 44.5°. (a) spatial distribution of MODIS color-coded FRP values for the selected fire region with overlaid OCO-2 ground pixel footprints (with black lines as boundaries). (b) Difference between the spectra of a solar background and fire pixel showing clear dual-peak potassium emission lines. c) PC-2 showing the potassium line at 770.1 nm. d) Correlation between MODIS FRP and the PC-2 scores with the PC-2 score threshold value set as 0.

lines rather than the K-line at 770.1 nm.

For both TROPOMI and OCO-2 instruments, we show that PCA effectively isolates the K-line signal from background sources of signal variance and that the results are sensitive to fire phase. Since the K-line PC scores are proportional to K-line radiances, correlation between PC scores and K-line PC scores and fire metrics also indicate correlation between these metrics and K-line radiance. In the TROPOMI data, the PC scores of the K-line PC correlate with FRP ($R = 0.55$, $\rho = 0.60$) and VLP ($R = 0.60$, $\rho = 0.67$). The correlation is stronger with VLP, indicating empirically that the observed K-line signal strength is tied to combustion phase. The OCO-2 results show moderate (R = 0.38, $\rho = 0.49$) correlation between the K-line PC and FRP, with the weakness compared to the TROPOMI case likely being due to the strong solar signal present in noon-time observations. These results may also be improved by performing atmospheric correction of the FRP observations.

When PCA is applied to the entire TROPOMI swath, the K-line PC detections correspond to the locations of FILDA-2 fire detections, showing that, indeed, the K-lines are indicative of biomass burning. A K-line PC score threshold of 0.05 successfully reduces the number of false detections to ~10%. Increasing this threshold also increases the average FRP and VEF of FILDA-2 fire detections containing the K-line detections, indicating that with proper thresholding, K-line data can be used quantitatively to isolate the most intense and flaming fires in VIIRS swath.

These results establish that K-lines can be detected under favorable conditions using TROPOMI and OCO-2 and show potential as a tool for characterizing fire phase and combustion efficiency. However, the quantitative relationships between satellite-observed K-line strength and fire phase and combustion efficiency is currently unknown and is left to future studies. As such, we consider this study an important proof-of-concept, rather than an outline of an operational product. Additionally, the extremely high spectral resolution of OCO-2 may allow the retrieval of additional information contained in the line shape, such as fire temperature. Further work is needed to establish the forward model to quantitatively relate the satellite-measured K-line intensity with the fire characteristics such as biomass burning rate and fire temperature.

CRediT authorship contribution statement

William Julstrom: Visualization, Methodology, Investigation, Formal analysis, Data curation, Conceptualization, Writing – original draft. **Jun Wang:** Supervision, Resources, Project administration, Methodology, Funding acquisition, Conceptualization, Writing – review & editing. **Meng Zhou:** Software, Methodology, Data curation.

Declaration of competing interest

The authors declare that they have no known competing financial interests or personal relationships that could have appeared to influence the work reported in this paper.

Acknowledgements

This work was supported in part by the Terra, Aqua, and Suomi National Polar-orbiting Partnership (SNPP) Program, National Aeronautics and Space Administration (NASA), under Award 80NNSC21L1976; by the Modeling and Analysis Program, NASA, under Award 80NSSC21K1494; by PYRocumulonimbus Experiment (INSPYRE) program, NASA, under Award 80NSSC26K0584, and by Public-Private-Partnership (P3) program in the University of Iowa.

Appendix A. Supplementary data

Supplementary data to this article can be found online at https://doi.org/10.1016/j.rse.2026.115542.

Data availability

TROPOMI L1B band 6 data are available at https://tropomi.gesdisc.eosdis.nasa.gov/data/S5P_TROPOMI_Level1B/S5P_L1B_RA_BD6_HiR.2/. VIIRS FILDA-2 can be found at https://www.earthdata.nasa.gov/data/catalog/lpcloud-vnp47mod-002. VIIRS SNPP geolocation data are located at https://ladsweb.modaps.eosdis.nasa.gov/archive/allData/5200/VNP03MOD/. OCO-2 L1B data were obtained from https://oco2.gesdisc.eosdis.nasa.gov/data/OCO2_DATA/OCO2_L1B_Science.11r/. Aqua MODIS MYD14 data can be found at https://ladsweb.modaps.eosdis.nasa.gov/archive/allData/61/MYD14/. Aqua MODIS geolocation data are located at https://ladsweb.modaps.eosdis.nasa.gov/archive/allData/61/MYD03/. The processed fire pixel data and PCA results can be found at https://doi.org/10.5281/zenodo.19636416.

References

Akagi, S.K., Yokelson, R.J., Wiedinmyer, C., Alvarado, M.J., Reid, J.S., Karl, T., Crounse, J.D., Wennberg, P.O., 2011. Emission factors for open and domestic biomass burning for use in atmospheric models. Atmos. Chem. Phys. 11, 4039–4072.

Amici, S., Wooster, M.J., Piscini, A., 2011. Multi-resolution spectral analysis of wildfire potassium emission signatures using laboratory, airborne and spaceborne remote sensing. Remote Sens. Environ. 115, 1811–1823.

Andreae, M.O., 2019. Emission of trace gases and aerosols from biomass burning – an updated assessment. Atmos. Chem. Phys. 19, 8523–8546.

Andreae, M.O., Merlet, P., 2001. Emission of trace gases and aerosols from biomass burning. Glob. Biogeochem. Cycles 15, 955–966.

Chen, X., Wang, J., Xu, X., Zhou, M., Zhang, H., Castro Garcia, L., Colarco, P.R., Janz, S. J., Yorks, J., McGill, M., Reid, J.S., de Graaf, M., Kondragunta, S., 2021. First retrieval of absorbing aerosol height over dark target using TROPOMI oxygen B band: algorithm development and application for surface particulate matter estimates. Remote Sens. Environ. 265.

Crisp, D., Pollock, H.R., Rosenberg, R., Chapsky, L., Lee, R.A.M., Oyafuso, F.A., Frankenberg, C., O'Dell, C.W., Bruegge, C.J., Doran, G.B., Eldering, A., Fisher, B.M., Fu, D., Gunson, M.R., Mandrake, L., Osterman, G.B., Schwandner, F.M., Sun, K., Taylor, T.E., Wennberg, P.O., Wunch, D., 2017. The on-orbit performance of the orbiting carbon Observatory-2 (OCO-2) instrument and its radiometrically calibrated products. Atmos. Meas. Tech. 10, 59–81.

Crutzen, P.J., Andreae, M.O., 1990. Biomass burning in the tropics: impact on atmospheric chemistry and biogeochemical cycles. Science 250, 1669–1678.

Crutzen, P.J., Heidt, L.E., Krasnec, J.P., Pollock, W.H., Seiler, W., 1979. Biomass burning as a source of atmospheric gases CO, H2, N2O, NO, CH3Cl and COS. Nature 282, 253–256.

Deng, W., Zhou, M., Wang, J., Xue, Z., Lu, Z., Chen, X., Zhang, H., Peterson, D.A., Hyer, E.J., da Silva, A.M., 2024. Advancing FRP retrieval: bridging theory and application. IEEE Trans. Geosci. Remote Sens. 62, 1–16.

Dennison, P.E., Roberts, D.A., 2009. Daytime fire detection using airborne hyperspectral data. Remote Sens. Environ. 113, 1646–1657.

Ding, Y., Vandervort, J.A., Freedman, R.S., Strand, C.L., Marley, M.S., Hanson, R.K., 2022. Collisional broadening and pressure shift of the potassium resonance doublets by nitrogen, helium, and hydrogen at high temperatures. J. Quant. Spectrosc. Radiat. Transf. 283.

Guanter, L., Bacour, C., Schneider, A., Aben, I., van Kempen, T.A., Maignan, F., Retscher, C., Köhler, P., Frankenberg, C., Joiner, J., Zhang, Y., 2021. The TROPOSIF global sun-induced fluorescence dataset from the sentinel-5P TROPOMI mission. Earth Syst. Sci. Data 13, 5423–5440.

Kaaret, P., Tammes, S., Wang, J., Scnnell, T., Linderman, M., Richey, C.H., Packard, C.M., Zhou, M., Fuller, C.A., 2022. On the potential of flaming hotspot detection at night via multiband visible/near-infrared imaging. Remote Sens. 14.

Kaiser, J.W., Heil, A., Andreae, M.O., Benedetti, A., Chubarova, N., Jones, L., Morcrette, J.J., Razinger, M., Schultz, M.G., Suttie, M., van der Werf, G.R., 2012. Biomass burning emissions estimated with a global fire assimilation system based on observed fire radiative power. Biogeosciences 9, 527–554.

Kaufman, Y.J., Justice, C.O., Flynn, L.P., Kendall, J.D., Prins, E.M., Giglio, L., Ward, D.E., Menzel, W.P., Setzer, A.W., 1998. Potential global fire monitoring from EOS-MODIS. J. Geophys. Res. 103, 32215–32238.

Magidimisha, E., Griffith, D.J., 2017. Remote optical observations of actively burning biomass fires using potassium line spectral emission. In: Fourth Conference on Sensors, MEMS, and Electro-Optic Systems.

Ononye, A., Vodacek, A., Kremens, R., 2005. Improved fire temperature estimation using constrained spectral unmixing. In: Remote Sensing for Field Users. Am. Soc. Photogram. Remote Sens., Pp. CD–ROM, Proc. 10th Biennial USDA Forest Service Remote Sensing Applications Conference. Salt Lake City, UT.

Owsley-Brown, F., Wooster, M.J., Grosvenor, M.J., Liu, Y., 2024. Can the remote sensing of combustion phase improve estimates of landscape fire smoke emission rate and composition? Atmos. Meas. Tech. 17, 6247–6264.

Reid, J.S., Hyer, E.J., Prins, E.M., Westphal, D.L., Zhang, J., Wang, J., Christopher, S.A., Curtis, C.A., Schmidt, C.C., Eleuterio, D.P., Richardson, K.A., Hoffman, J.P., 2009. Global monitoring and forecasting of biomass-burning smoke: description of and

lessons from the fire locating and modeling of burning emissions (FLAMBE) program. IEEE J. Sel. Top. Appl. Earth Observ. Remote Sens. 2, 144–162.
Sorvajarvi, T., DeMartini, N., Rossi, J., Toivonen, J., 2014. In situ measurement technique for simultaneous detection of K, KCl, and KOH vapors released during combustion of solid biomass fuel in a single particle reactor. Appl. Spectrosc. 68, 179–184.
Vodacek, A., Kremens, R., Fordham, A.J., Vangorden, S.C., Luiai, D., Schott, J.R., 2002. Remote optical detection of biomass burning using a potassium emission signature. Int. J. Remote Sens. 23, 2721–2726.
Waigl, C.F., Prakash, A., Stuefer, M., Verbyla, D., Dennison, P., 2019. Fire detection and temperature retrieval using EO-1 Hyperion data over selected Alaskan boreal forest fires. Int. J. Appl. Earth Obs. Geoinf. 81, 72–84.
Wang, J., Roudini, S., Hyer, E.J., Xu, X., Zhou, M., Castro Garcia, L., Reid, J.S., Peterson, D.A., da Silva, A.M., 2020. Detecting nighttime fire combustion phase by hybrid application of visible and infrared radiation from Suomi NPP VIIRS. Remote Sens. Environ. 237.
van der Werf, G.R., Randerson, J.T., Giglio, L., van Leeuwen, T.T., Chen, Y., Rogers, B.M., Mu, M., van Marle, M.J.E., Morton, D.C., Collatz, G.J., Yokelson, R.J., Kasibhatla, P. S., 2017. Global fire emissions estimates during 1997–2016. Earth Syst. Sci. Data 9, 697–720.
Zhou, M., Wang, J., Garcia, L.C., Chen, X., da Silva, A.M., Wang, Z.S., Román, M.O., Hyer, E.J., Miller, S.D., 2023. Enhancement of nighttime fire detection and combustion efficiency characterization using Suomi-NPP and NOAA-20 VIIRS instruments. IEEE Trans. Geosci. Remote Sens. 61.